



Preparation, optimization, and in vitro–in vivo evaluation of sorafenib-loaded polycaprolactone and cellulose acetate nanofibers for the treatment of cutaneous leishmaniasis

Mahsa Alemomen¹ · Somayeh Taymouri¹ · Sedigheh Saberi² · Jaleh Varshosaz¹

Accepted: 3 October 2022 / Published online: 12 October 2022
© Controlled Release Society 2022

Abstract

The most common form of leishmaniasis is cutaneous leishmaniasis (CL). The major difficulties in the treatment of leishmaniasis include emergence of resistance, toxicity, long-term treatment, and the high cost of the current drugs. Although the therapeutic effect of sorafenib (SF) has been demonstrated in both in vitro and in vivo models of *Leishmania* infection, the therapeutic applications are limited due to severe drug-related toxicity; this is, in turn, due to non-specific distribution in the body. Thus, topical delivery has the advantage of the site directed delivery of SF. This research study evaluated SF-loaded hybrid nanofibers (NFs) which were composed of polycaprolactone (PCL) and cellulose acetate (CA) for the CL topical treatment. Accordingly, SF-loaded hybrid NFs were prepared using the electrospinning method. Formulation variables including total polymer concentration, drug/polymer ratio, and CA concentration were optimized using a full factorial design. The prepared SF-loaded NFs were then characterized for morphology, diameter, encapsulation efficiency (EE)%, drug loading (DL) %, and percentage of release efficiency during a 24-h period (RE_{24h}%); the mechanical characteristics were also considered. The physical state of the drug in the optimized NF was evaluated by the X-ray diffraction analysis. Finally, its in vivo efficacy was determined in *L. major*-infected mice. The optimized formulation had a smooth, cylindrical, non-beaded shape fiber with a diameter of 281.44 nm, EE of 97.96%, DL of 7.48%, RE of 51.05%, ultimate tensile strength of 1.08 MPa, and Young's moduli of 74.96 MPa. The XRD analysis also demonstrated the amorphous state of SF in NF. Further, the in vivo results displayed the higher anti-leishmanial activity of the SF-loaded hybrid NF by efficiently healing lesion and successfully reducing the parasite burden. This, thus, indicated the potential of the clinical capability of the SF-loaded hybrid NF for the effective treatment of CL.

Keywords Cutaneous leishmaniasis · Sorafenib · Nanofibers · Cellulose acetate · Electrospinning · Parasite burdens

Introduction

Leishmaniasis is a major global health problem caused by different species of parasitic protozoa belonging to genus *Leishmania*, which are injected into the skin by the bite of the infected female sand fly of the genus *Phlebotomus*

during blood feeding [1]. Leishmaniasis parasitic infections appear in several distinct clinical forms, depending on several factors related to parasites and the immunological status of the host [2]. There are three main forms of leishmaniasis. The first form is cutaneous leishmaniasis (CL), characterized by a number of localized skin lesions at the infection site with various manifestations ranging from small nodules to large plaques, as well as ulcers. The second one includes mucocutaneous leishmaniasis, typically accompanied by destructive mucosal infections [3]. The third one is visceral leishmaniasis (Kala-azar), the most serious and fatal form of the disease characterized by the presence of parasites in the spleen, liver, and bone marrow and systemic infection symptoms [3]. CL is the most common form of leishmaniasis with the annual incidence of 1.5 million new cases that are caused by more than 15

✉ Somayeh Taymouri
s_taymouri@pharm.mui.ac.ir

¹ Department of Pharmaceutics, School of Pharmacy and Novel Drug Delivery Systems Research Centre, Isfahan University of Medical Sciences, PO Box 81745-359, Isfahan, Iran

² Department of Parasitology and Mycology, School of Medicine, Isfahan University of Medical Sciences, Isfahan, Iran

species of *Leishmania* [4]. While CL is commonly regarded as a self-healing disease with a low incidence of mortality, ulcerative lesions are often on the body's exposed parts and the parts not treated can change into disfiguring scar, as well as life-long stigmas, thus leading to psychological suffering and the patients' affected quality of life [5]. In few cases, insufficient treatment of a primary CL lesion may pose a risk to an individual for mucocutaneous leishmaniasis later development [2]. The drugs currently used for the treatment of leishmaniasis are pentavalent antimony compounds as the first-line and amphotericin B and pentamidine as the second-line anti-leishmanial regimen. However, the high cost, long treatment times, the need for frequent hospitalization, the emergence of drug resistance, especially in HIV patients, and variable side effects are some issues associated with such treatments [6, 7]. Sorafenib (SF) is a multi-kinase inhibitor inhibiting tumor-cell proliferation and tumor angiogenesis by targeting RAF kinase, platelet-derived growth factor, vascular endothelial growth factor (VEGF) receptor kinases, and c-Kit receptor. It is used in treating advanced renal cell carcinoma and unsectable hepato-carcinoma [8]. In addition, SF shows a remarkable anti-parasitic activity in the *in vitro* and *in vivo* models of *Leishmania* infection [9, 10]. Tablet formulation which has 200 mg SF can be obtained in markets for oral use; however, therapeutic application of SF is restricted due to low oral bioavailability (38–49%) and high inter-subject variability resulting from its unfavored biopharmaceutical features including poor solubility and first-pass metabolism and serious drug-associated toxicity owing to non-specific distribution in the body, like diarrhea, hand–foot skin reaction, alopecia, anorexia, and loss of weight as well as abdominal pain [11, 12]. Since CL is a skin disease, development of a formulation for the topical treatment of CL may alleviate, at least partly, the mentioned problems. Topical treatment offers numerous advantages when compared with oral administration, like avoiding the first pass metabolism, the total needed dose minimization owing to the drug delivery to the particular action site, and decreased adverse reaction incidence as well as cost [13, 14]. In the recent years, a wide variety of systems have been developed for topical drug delivery applications; these include sponges, foams, wafers, hydrogels, films, membranes, and nanofibers. Among these systems, nanofibers (NFs) have received special attention in biomedical fields due to their extraordinary properties such as ultrafine structure, simplicity of production, high surface area to volume ratio, porous matrix, high oxygen permeability, and adjustable drug release profile [15–18]. As it can well mimic the natural extra cellular matrix (ECM), NFs could create a structural support for cell attachment, growth, and migration on the wound region, thus accelerating the creation of new tissue and replacing it with the damaged one in the body [19]. Several studies on the use of

nanofibrous systems for the delivery of anti-leishmaniasis are available in the literature. For example, nanofibrous systems were loaded with glucantime [20] and berberine [21] and then used for the treatment of leishmaniasis. Polycaprolactone (PCL) is an aliphatic polyester approved by Food and Drug Administration (FDA) and extensively used in biomedical areas because of its biocompatibility, biodegradability, low-cost, non-toxicity, and good mechanical properties; however, the major limitation of PCL is its hydrophobic properties, which might lead to the unsatisfactory release of the hydrophobic drug. In addition, PCL does not have cell recognition sites due to its hydrophobic nature, thus limiting cell adhesion and proliferation [22, 23]. Blending PCL with a hydrophilic polymer like cellulose acetate (CA) may considerably improve its characteristics, such as hydrophilicity and cell binding capability [24, 25]. CA is an acetate ester form of cellulose. Due to its biocompatibility, biodegradability, mechanical performance, low cost, availability, water absorption ability, cell binding ability, and regenerative properties, this polymer has numerous biomedical applications in drug delivery systems, tissue engineering, and wound dressing [26, 27]. According to the above, in this study, SF-loaded PCL-CA electrospun mats were fabricated and optimized using a full factorial design. Then, the morphology, diameter, encapsulation efficiency (EE)%, drug loading (DL) % and release efficiency percentage over 24 h (RE_{24h}%), and the mechanical characteristics of the electrospun NF were assessed. In the next stage, anti-leishmaniasis of the mats were investigated in *L. major*-infected mice.

Materials and methods

Materials

SF was supplied by Parsian Pharmaceutical Co (Iran); CA (MW = 30 kDa; acetyl content = 39.7% (w/w) and PCL (Mw = 80,000 Da) were purchased from Sigma Chemical Co. (USA); dimethyl formamide (DMF), chloroform, and dimethyl sulfoxide (DMSO) were from Merck (Germany). Roswell Park Memorial Institute 1640 medium (RPMI-1640), Novy-MacNeal-Nicolle medium (NNN), fetal bovine serum (FBS), trypsin/EDTA, and penicillin/streptomycin were purchased from Gibco Company (USA). All other used chemicals and solvents were of analytical reagent grade.

Animals

Female BALB/c mice (aged 6–8 weeks, weighting 25 ± 5 g) were purchased from Pasteur Institute of Iran. The animals were kept in a light-controlled animal house (12-h light/12-h

Table 1 Different factors and their levels investigated by full factorial design in production of SF-loaded NF

Independent variables	Symbol	Levels	
		I	II
Polymer content (% w/v)	A	12	16
Drug/Polymer ratio (%w/w)	B	5	10
CA content (% w/w with respect polymer content)	C	40	80

dark cycle) of pharmacy school with a temperature of 24 ± 1 °C, and humidity of $55 \pm 5\%$. The animals had free excess to food and water. All experiments were performed as per the guidelines directed by the Ethical Committee of Isfahan University of Medical Sciences in regard to the care and use of laboratory animals (ethics code number # IR.MUI.RESEARCH.REC.1399.489).

Fabrication of SF-loaded NF

An appropriate amount of PCL and CA at different weight ratios (20:80 and 60:40) were dissolved in a mixed solvent (chloroform/DMF, 7:3 by volume) at room temperature and stirred until a homogeneous solution was obtained. The total polymer concentration was 12 and 16% (w/v). Then, SF powder (5–10% w/w with respect to the polymer content) was added to polymer solution. Each of solution was introduced into a 1 ml plastic syringe with a 27-gauge needle. Plastic syringe was put in the electrospinning device (Fanavar Nano Meghyas Ltd., Co., Tehran, Iran), and electrospinning was performed under controlled conditions such as an applied voltage of 13 kV, the tip-to-collector distance of 17 cm, and solution

flow rate of 0.3 ml/h. The rotating drum surface was covered with aluminum foil, and nanofiber samples were collected on the aluminum foil sheet attached on the surface of a rotating drum and stored in desiccator for further characterization.

Experimental design

A 2^3 full factorial design was used for optimization of SF-loaded NF and to investigate the effect of total polymer concentration (% w/v), drug/polymer ratio (% w/w), and cellulose acetate concentration (% w/v, with respect to total polymer concentration) as the main independent variables on different properties of NF. The minimum and maximum levels of studied parameters as shown in Table 1 were obtained from preliminary experiments. The compositions of different prepared NFs are summarized in Table 2. The investigated responses chosen were morphology, diameter, EE %, DL %, RE_{24h}%, ultimate tensile strength (UTS), and Young's modulus. Design Expert® software (version 11, USA) was used to analyze the statistical significance and create 3D response surface plots.

Characterization of NF

The diameter and morphology of electrospun NF

Scanning electron microscopy (SEM, FEI Co, USA) operating at 15 kv was used to examine the surface morphology of SF-loaded electrospun NF. For this end, each sample was sputter coated with gold and then observed with SEM. Image J software was used to measure the average diameter of the NF mats by analysis of SEM images. The mean values were calculated from at least 50 measurements.

Table 2 Composition and viscosity of different formulated SF-loaded NF

Formulations	Total polymer concentration (%w/v)	CA amount (%w/w with respect to polymer amount)	SF amount (%w/w with respect to polymer amount)	Viscosity (centipoise)
P ₁₂ R ₀ D ₅	12	0	5	950
P ₁₂ R ₄₀ D ₅	12	40	5	691
P ₁₂ R ₈₀ D ₅	12	80	5	544
P ₁₂ R ₀ D ₁₀	12	0	10	712
P ₁₂ R ₄₀ D ₁₀	12	40	10	598
P ₁₂ R ₈₀ D ₁₀	12	80	10	461
P ₁₆ R ₀ D ₅	16	0	5	1178
P ₁₆ R ₄₀ D ₅	16	40	5	925
P ₁₆ R ₈₀ D ₅	16	80	5	810
P ₁₆ R ₀ D ₁₀	16	0	10	1052
P ₁₆ R ₄₀ D ₁₀	16	40	10	799
P ₁₆ R ₈₀ D ₁₀	16	80	10	701

EE% and DL % determination

To determine the EE % and DL %, a piece of electrospun membrane ($1 \times 1.5 \text{ cm}^2$) was dissolved in 1 ml of DMSO and then analyzed in an ultraviolet (UV) visible spectrophotometer (UV-mini 1240, Shimadzu, Kyoto, Japan) at $\lambda_{\text{max}} = 270 \text{ nm}$ after proper dilution. The following equations were used for calculation of EE % and DL%

$$EE\% = \frac{W_d}{W_t} \times 100 \quad (1)$$

$$DL\% = \frac{W_d}{W_n} \times 100 \quad (2)$$

where W_d , W_t , and W_n indicate the weight of SF entrapped into fibers mat, the weight of SF used to prepare the fiber mat, and weight of the drug-loaded fiber mat, respectively.

In vitro release studies

Release of the drug from formulated fiber was evaluated by using Franz diffusion cell. A piece of each electrospun membrane with dimension of $2.5 \times 2.5 \text{ cm}^2$ was placed on the surface of cellulose acetate membrane mounted between donor and receptor compartments of cells. The receptor was filled with 30 ml PBS:ethanol (50:50 v/v) and was stirred at 500 rpm. The temperature in the Franz diffusion cell was $37 \text{ }^\circ\text{C} \pm 0.5 \text{ }^\circ\text{C}$. At predefined time points (1, 2, 3, 4, 5, 8, and 24 h), samples were taken from release medium and then replaced with fresh medium. The released drug was determined with UV spectrophotometer (Shimadzu®, Japan) at 265 nm. The percentage cumulative amount of drug released was determined from in vitro release profile. To compare release medium, $RE_{24h}\%$ was determined by using following equation

$$RE_{24h}\% = \frac{\int_0^t y \cdot dt}{y_{100} \cdot t} \times 100 \quad (3)$$

where $Y \cdot dt$ represents the area below the release curve up until the time, t , and $y_{100} \cdot t$ indicates the rectangle area defined at the same time by 100% release.

Release kinetic study

To study drug release kinetics, the drug release data from the optimized sample were fitted to following kinetic models

$$\text{Zero order : } (Q_t/Q_\infty = kt) \quad (4)$$

$$\text{First order : } (\ln(1 - Q_t/Q_\infty) = -kt) \quad (5)$$

$$\text{Baker - Lonsdale : } 3/2[1 - (1 - Q_t/Q_\infty)^{2/3}] - Q_t/Q_\infty = kt \quad (6)$$

$$\text{Higuchi : } Q_t/Q_\infty = kt^{1/2} \quad (7)$$

$$\text{Korsmeyer-Peppas model : } (Q_t/Q_\infty = kt^n) \quad (8)$$

where k is the drug release rate constant for each model, Q_t/Q_∞ denotes the fraction of drug release at time (t), and n is release exponent used to determine mechanism of drug release. Accordingly, $n \leq 0.45$ is an indication of Fickian diffusion mechanism. If $0.45 < n < 0.89$, the drug release follows a non-Fickian model indicating a combination of the diffusion from the polymeric matrix and the surface erosion of the polymer are involved in drug release and when $n = 0.89$ and $n > 0.89$, drug release follows zero-order kinetics and super Case-II transport, respectively [28]. The best fit model was determined by higher correlation values.

Mechanical properties of electrospun membrane

The mechanical properties of nanofiber membranes in terms of Young's moduli and UTS values were measured using a SANTAM instrument (SANTAM Co, Iran). The samples ($1 \text{ cm} \times 3 \text{ cm}$) were stretched at a speed of 10 mm/min.

Fourier-transform infrared spectra (FTIR)

The FTIR spectrum of CA, PCL, and SF was measured by applying a KBr disk using FTIR spectrophotometer (JASCO, Model 6300, Japan). Attenuated total reflection Fourier-transform infrared spectroscopy (ATR-FTIR, JASCO, Model 6300, Japan) was used to evaluate optimized NF with and without SF.

X-ray diffraction (XRD) analysis

The XRD patterns of SF, CA, PCL, and optimized nanofibers with and without SF were investigated using XRD diffractometer (Bruker, Germany) using $\text{CuK}\alpha$ radiation at 40 kV and 40 mA in 2θ range of 5° to 80° .

Skin permeation

Ex vivo skin permeation investigation was done for the SF-loaded PCL-CA composite NF and SF suspension in Franz diffusion cells which were fitted with a diffusion area equal to 4.9 cm^2 and a reservoir capacity of 30 ml. The shaving of the rat skin was done following its sacrifice by CO_2 ; then, excising and rinsing were carried out using physiological saline. The obtained skin samples were then subjected to clamping between the receptor and donor of the

Franz diffusion cell. The receptor compartment was then filled with PBS:ethanol (50:50 v/v), which was stirred in a constant manner by applying the magnetic stirrer during the experiment. The buffer's temperature was then kept at the $37\text{ }^{\circ}\text{C} \pm 0.5\text{ }^{\circ}\text{C}$ range by applying a re-circulating water bath. SF-loaded PCL-CA composite NF and SF suspension which contained $300\text{ }\mu\text{g}$ SF were put on the skin's surface in the donor compartment, separately. At time intervals previously determined (2, 3, 4, 5, 8, and 24 h), withdrawal of 1 ml samples from the receiver compartment was done; then, they were replaced with the fresh medium. The SF amount was subjected to analysis through UV spectrophotometry at 265 nm. Each of the tests was carried out three times. Finally, for the evaluation of permeability, the SF mean cumulative amount, which permeated the rat skin's surface area per unit, was plotted against time.

Efficacy studies in *L. major*-infected BALB/C mice

Leishmania major (*L. major*) promastigotes (MRHO/IR/75/ER) were obtained from the Department of Parasitology & Mycology, Isfahan University of Medical Sciences, Iran. This parasite was first cultured in Novy-McNeal-Nicol (NNN) medium and then this continued in RPMI1640 media enriched with 10% fetal bovine serum (FBS), penicillin (100 IU/ml), and streptomycin (100 $\mu\text{g}/\text{ml}$). After promastigotes reached their metacyclic phase, 100 μl RPMI1640 containing 2×10^6 metacyclic promastigotes were injected intradermally at the base of the animal's tail. After 2 weeks, when lesions were emerged, the diameter of lesion was measured and then mice were randomly divided into 5 groups. Group 1 treated orally with SF (50 mg/kg), group 2 received topically SF-loaded PCL-CA hybrid NF (50 mg/kg) and group 3 received topically drug-free PCL-CA composite NF with the same amount of polymer in SF-loaded hybrid NF. Group receiving normal saline was used as negative control and group getting Glucantime (100 mg/kg) intraperitoneally was used as positive control. The treatments were carried out every day for 14 days. During treatment, the lesion size (in mm) was determined with a Kulis vernier by recording average diameters in horizontal and vertical directions

$$\text{Lesion size reduction \%} = \left(\frac{\text{Lesion size on day [0]} - \text{Lesion size on day[n]}}{\text{Lesion size on day[0]}} \right) \times 100 \quad (9)$$

where n is the number of days.

At the end of study, animals were sacrificed by CO_2 , and livers and spleens of mice were removed and weighed. To determine parasite burdens in spleens and livers, multiple smears were prepared and then stained with Giemsa. Then, the total number of amastigotes per organ was calculated as the

organ weight (in milligrams) \times number of amastigotes per 1000 nucleus [29]. Skin lesions were also excised in normal saline and SF-loaded hybrid NF treated groups and then stained with hematoxylin and eosin (H and E staining). These sections were then evaluated under optical microscope (Olympus, Tokyo, Japan) to determine parasite density. Furthermore, the body weight of each of the mice under study was determined at the beginning and in the end of study.

Results and discussion

In the present study, SF-loaded PCL NF mats were generated using the electrospinning process. As shown in Fig. 1, SF-loaded PCL NF mats were a smooth beaded-free cylindrical fiber with diameters in a nanometer size ranging from 580.64 to 885.95 nm. EE% and DL% of SF-loaded PCL NF mats were also found to be in the range of 71.57–92.58% and 4.47–8.87%, respectively. The prepared NF showed a slow release rate (Fig. 2). In addition, the production of smooth and bead-free fibers with the electrospinning of CA/SF solutions was impossible even for small amounts of the drug. To solve these problems, CA was added to PCL to produce a membrane for the delivery of SF. Regarding the effect of formulation parameters on the characteristics of the fiber, formulation variables including total polymer concentration, drug/polymer ratio, and CA concentration were optimized using the full factorial design. The data obtained from the evaluation of different experimental runs, as generated by the full factorial design of the Design expert software, are summarized in Table 3. The results obtained from the ANOVA of the considered responses can be observed in Table 4. Contribution effect % of each parameter and their combination on various responses can be seen in Fig. 3. The 3-D response surface plots depicting the effect of the predetermined factors on the studied responses are shown in Fig. 4. In addition, polynomial equations generated to illustrate the effect of independent variables on the responses in a better way are shown in Eqs. 10–15. In the polynomial equation, the direct relation is denoted by the positive coefficient, whereas the negative one indicates the inverse relationship between the independent variables and dependent responses.

Morphological characterization of the SF-loaded NF

The SEM images of different SF-loaded PCL-CA composite NF membranes are shown in Fig. 1. As can be seen, ribbon-like, interconnected, bead less, and randomly oriented NF with diameters in nanoscales were formed.

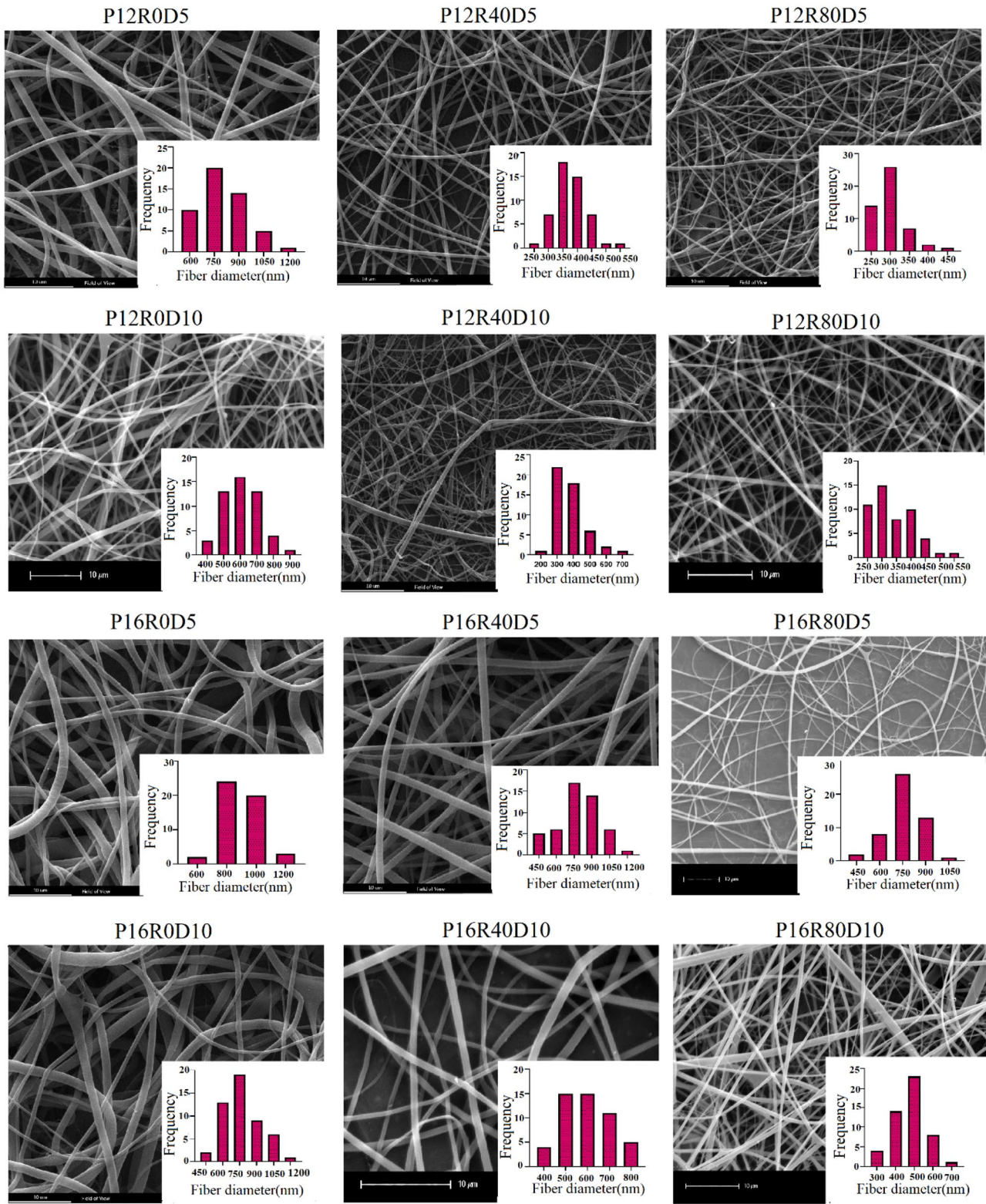


Fig. 1 SEM images of NF containing SF

Fig. 2 SF release profiles from different NF. Each point represents the mean \pm SD of three experiments

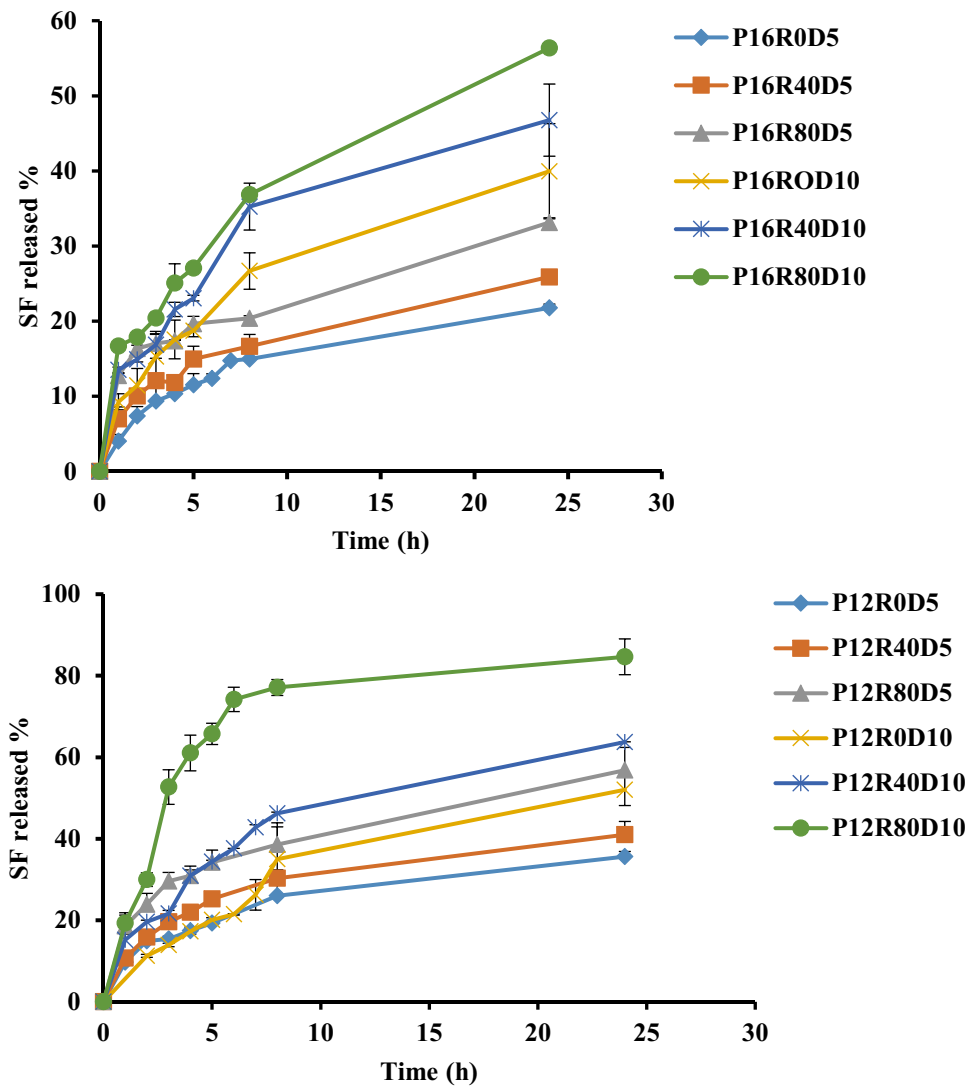


Table 3 Characterization of SF-loaded NF (means \pm S.D.; $n=3$)

Formulations	Diameter (nm)	Encapsulation efficiency%	Drug loading (%)	Release efficiency (%)	Ultimate tensile strength (MPa)	Young's modulus (MPa)
P12R0D5	799.68 \pm 125.61	92.58 \pm 5.08	5.16 \pm 0.28	26.17 \pm 0.30	0.68 \pm 0.02	5.60 \pm 0.06
P12R40D5	376.03 \pm 53.82	99.94 \pm 2.48	5.99 \pm 0.14	30.60 \pm 1.86	1.18 \pm 0.04	30.37 \pm 1.54
P12R80D5	301.94 \pm 41.86	98.22 \pm 4.44	5.27 \pm 0.23	41.36 \pm 4.25	1.71 \pm 0.19	114.49 \pm 3.61
P12R0D10	580.64 \pm 103.05	71.57 \pm 5.17	8.43 \pm 0.61	34.55 \pm 4.69	2.27 \pm 0.13	3.96 \pm 0.14
P12R40D10	369.58 \pm 88.45	97.71 \pm 0.71	11.07 \pm 0.8	46.04 \pm 0.11	0.19 \pm 0.01	5.36 \pm 0.30
P12R80D10	284.88 \pm 72.24	95.96 \pm 1.82	10.01 \pm 0.19	67.78 \pm 7.96	0.39 \pm 0.06	29.94 \pm 1.76
P16R0D5	885.95 \pm 137.77	72.99 \pm 5.27	4.47 \pm 0.32	15.47 \pm 0.12	2.84 \pm 0.22	3.56 \pm 0.06
P16R40D5	782.02 \pm 162.95	87.16 \pm 0.36	5.24 \pm 0.02	19.36 \pm 0.92	0.22 \pm 0.02	5.75 \pm 0.06
P16R80D5	744.5 \pm 113.47	71.46 \pm 4.68	4.92 \pm 0.32	23.39 \pm 0.20	1.22 \pm 0.17	64.46 \pm 1.86
P16R0D10	764.34 \pm 159.93	74.12 \pm 2.32	8.87 \pm 0.27	27.67 \pm 3.50	1.56 \pm 0.10	3.05 \pm 0.15
P16R40D10	594.08 \pm 110.02	79.21 \pm 1.99	12.08 \pm 0.30	34.25 \pm 2.98	0.72 \pm 0.07	20.76 \pm 0.98
P16R80D10	475.1 \pm 79.67	61.95 \pm 5.04	9.75 \pm 0.35	38.97 \pm 0.20	0.35 \pm 0.05	11.14 \pm 1.30

Table 4 Results of ANOVA analysis of responses

Parameters	Drug loading % <i>p</i> value	Encapsulation efficiency % <i>p</i> value	Release efficiency % <i>p</i> value	Diameter <i>p</i> value	Ultimate tensile strength <i>p</i> -value	Young's modulus <i>p</i> -value
Model	0.0045	0.0011	0.0456	0.0030	0.0424	0.0591
A	-	0.0003	0.0233	0.0012	0.0634	0.0716
B	0.0010	0.0050	0.0218	0.0030	0.0226	0.0379
C	0.0217	0.0018	0.0628	0.0046	0.0440	0.0355
AB	0.1090	0.0142	-	0.0034	0.0313	0.0783
AC	-	0.0028	0.1601	-	-	0.0934
BC	0.0708	-	0.3950	0.0159	0.0356	0.0438
ABC	0.1286	-	-	0.0206	0.0581	-

A: polymer content (% w/v); B: drug/polymer ratio (%w/w); C: CA content (% w/w with respect polymer content)

Diameter

Diameter is a key parameter affecting the drug release profile from NF. Fibers with a smaller diameter have a shorter diffusion passage length along with a greater surface area for effective mass transfer. Average diameters of the prepared NF were in the range of 284.88 to 885.95 nm. Equation 10 describes the relationship between the diameter of NF and the independent variables.

$$\text{Diameter} = 491.02 + 157.91 A - 60.11 B - 39.41 C - 54.23 AB - 11.51 BC - 8.86 ABC \quad (10)$$

where A is the polymer content (% w/v), B is the drug/polymer ratio (%w/w), C is the CA content (% w/w with respect polymer content), and AB and BC are the combined effect of the two factors.

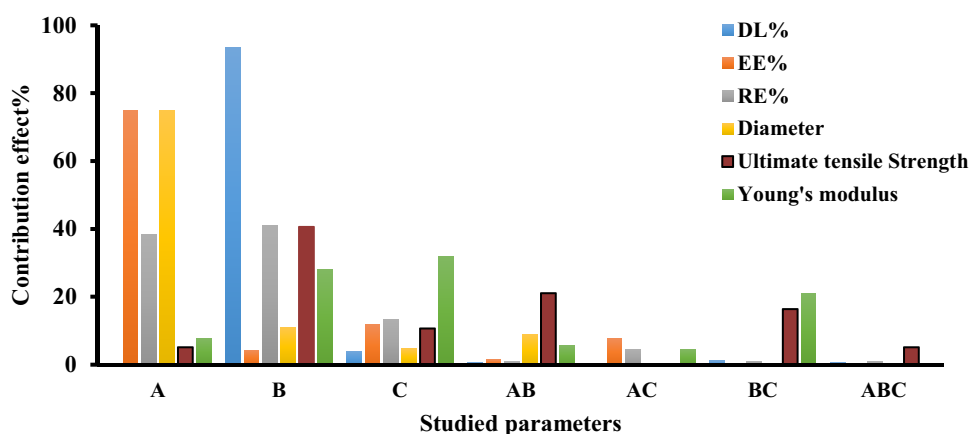
According to the polynomial Eq. 10 and Fig. 3, the total polymer concentration had a greater influence on the fiber diameter (*p*-value < 0.05); as such, the fiber diameter was increased with the rise of the polymer concentration, possibly owing to its influence on viscosity (Fig. 4a) which

was in accordance with the data shown in Table 3. Our results were, thus, in a good agreement with the previous findings, showing that the diameter of fiber depends on the viscosity of solution and increases with the rise of it [23, 30]. The increased viscosity of the solution with the higher polymer concentration causes higher viscoelastic forces that can resist axial stretching during whipping, resulting in a thicker fiber [31]. An enhancement in the SF/polymer ratio and CA concentration resulted in the depletion of the fiber diameter (*p*-value < 0.05, Fig. 4b). This could be explained in terms of the reduction of viscosity, which might be due to SF and CA molecules acting as a plasticizer for PCL chains [32, 33].

Drug EE% and DL %

As shown in Table 3, EE% and DL% of the SF-loaded NF ranged from 61.95 to 99.94% and 4.92 to 12.08%, respectively. Equations 11 and 12 describe the relationship between the EE% and DL% of the nanofibers and independent variables.

Fig. 3 Contribution effect % of each parameter and their combination on various responses. A: polymer content, B: drug/polymer ratio, C: CA content. AB, AC, AD, and BC are combined effect of two factors and ABC is combined effect of three factors



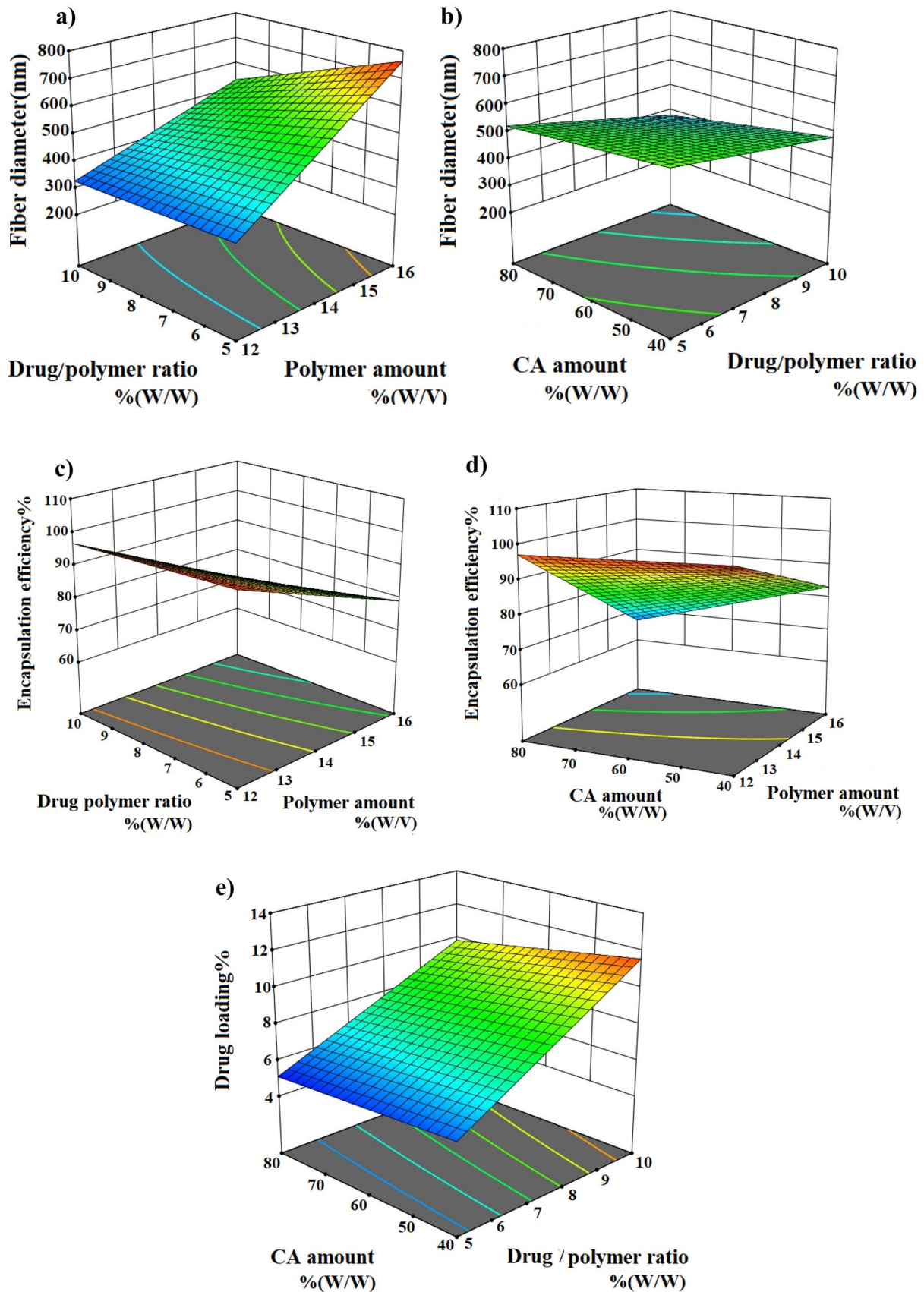


Fig. 4 3-D response surface plots depicting the effect of predetermined factors on studied responses

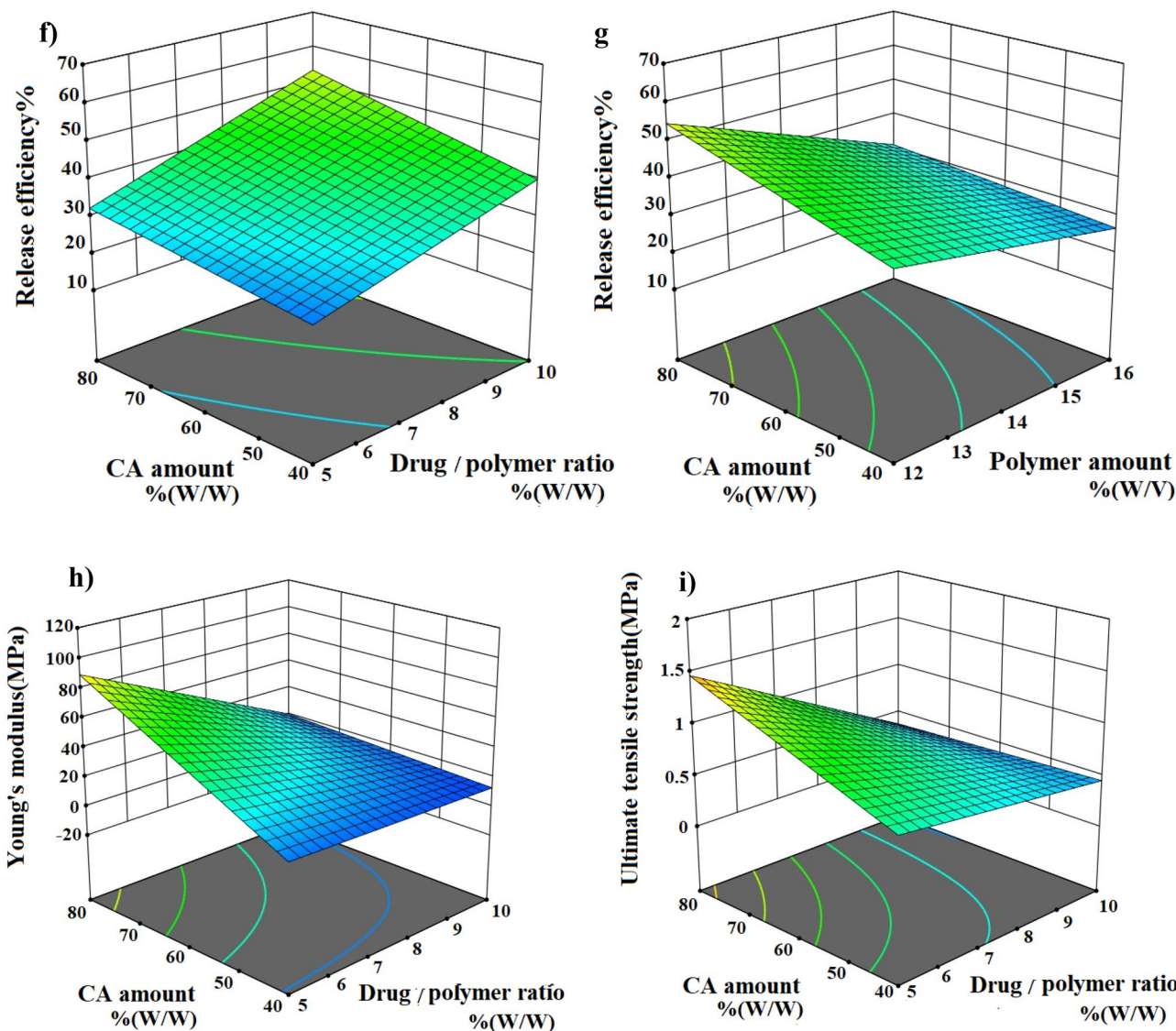


Fig. 4 (continued)

$$EE \% = 86.45 - 11.51 A - 2.75 B - 4.55 C - 1.62 AB - 3.69 AC \tag{11}$$

$$DL\% = 8.05 + 2.69 B - 0.555 C + 0.231 AB - 0.295 BC + 0.209 ABC \tag{12}$$

According to polynomial Eq. 11, all studied factors had an inverse effect on EE. Also, the higher coefficient value of the polymer concentration indicated that it had a more significant effect on EE, which was followed by the CA concentration and drug/polymer ratio (Fig. 3). It was also found that the EE % of the SF-loaded PCL-CA NF was decreased with raising the polymer concentration (p -value < 0.05, Fig. 4c). The lower capability of NF to encapsulate SF at higher polymer concentration might be due to its higher viscosity, which could negatively affect the miscibility of the drug in the polymer solution, thus resulting in the lower EE %.

Moreover, the reduction of EE with the rise of the drug/polymer ratio and concentration of CA (Fig. 4c, d) could be due to a substantial reduction in the diameter (p -value < 0.05). As reported in the literature, thicker fibers provide a higher EE due to more space to entrap drug molecules [23, 34]. DL%, which ranged from 4.92 to 12.08%, was mainly influenced by the drug/polymer ratio and cellulose acetate concentration (p -value < 0.05, Fig. 3). Increasing the drug/polymer ratio caused DL% to rise, thus indicating that there was more drug per unit weight of NF, which was expected with increasing the drug/polymer ratio (p -value < 0.05, Fig. 4e); meanwhile, elevating the CA concentration led to the decrease of the DL% of NF (p -value < 0.05, Fig. 4e). Such an adverse impact could be attributed to the decrease of the entrapped drug with increasing this variable.

In vitro release studies

Figure 2 displays the release profiles of SF from PCL NF with or without CA. As can be seen, the SF-loaded NF exhibited a biphasic release profile with an initial rapid release followed by a second sustained phase. The initial burst phase was due to the drug associated with the surface. The second slower release phase was obviously controlled by the diffusion of the drug entrapped inside the NF. A similar release pattern has also been reported by other researchers [35, 36]. To compare the profiles of drug release, RE % was calculated; the higher RE %, the faster the drug release rates. The measured RE was in the range of 19.36 to 67.78%. It was also found that the SF release rate of PCL-CA NF was higher than that of PCL NF, which could be attributed to the decrease in the hydrophobicity of the scaffold due to the hydrophilic nature of CA [26].

Equation 13 describes the effect of the independent variables on the RE% of the SF-loaded PCL/CA NF.

$$RE\% = 37.72 - 8.73 A + 9.04 B + 5.16 C - 2.97 AC + 1.46 BC \quad (13)$$

Figure 3 represents that the drug/polymer ratio was the most important parameter affecting RE_{24h}%. As indicated in Eq. 13 and Fig. 4f, g, the linear term of the drug/polymer ratio had a positive effect on the RE_{24h}% of NF, whereas the linear terms of the total polymer concentration had a negative one (p -value < 0.05). Changes in RE_{24h}% with these variables, e.g., a decrease in the release rate with increasing the polymers' concentration from 12 to 16%, could be due to their effects on the NF diameter. An inverse correlation between the fiber diameter and the release rate was also found [37]. The increased length of diffusion pathways with raising the fiber diameter could be the cause of the decrease in the release rate. A similar trend was also found with poly vinyl alcohol-polyvinyl pyrrolidone blend fibers fabricated by Kaur et al. [38] for the delivery of granisetron hydrochloride. The increase in RE with the rise of the drug/polymer ratio could also be due to the migration of more drug to the surface or near the surface of NF during the electrospinning process, as evidenced by the higher burst release from fibers. This is also shown in Fig. 2. When the drug loading was higher, less polymer per unit weight of NF was available to delay the SF release. The pore formed with the SF release promoted more rapid release of SF from NF [39]. As a result, the exposure and diffusion of SF to the release medium became higher, leading to a faster drug release rate. Similarly, Zamani et al. [40] found that increasing the metronidazole content in the polycaprolactone NF raised the drug release rate. Although not significant, the higher amount of CA favored the higher values of RE (p -value > 0.05, Fig. 4g) due to the hydrophilicity of CA, as described above. In the study conducted by Ramos et al.

[41] and Zhijiang et al. [24], with raising CA concentrations in PCL-CA and poly(hydroxybutyrate)/CA blend fibers, the water contact angle was decreased due to the increase in the hydrophilicity of the scaffold. This increased hydrophilicity could be desirable for the promotion of the more rapid hydration of the polymer, which could result in a faster drug release rate from NF.

Mechanical analysis of the electrospun NF membranes

Mechanical features are important for dressing applications since they determine how long the formulation integrity can last against environmental stresses during the healing process. The values for the UTS and Young's modulus are summarized in Table 3. The following equations show the relationship between Young's modulus and the UTS of the electrospun SF-loaded hybrid NF and the studied variables:

$$\text{Young's modulus} = 35.29 - 9.76 A - 18.48 B + 19.72 C + 8.91 AB - 7.45 AC - 15.98 BC \quad (14)$$

$$\text{UTS} = + 0.7503 - 0.1193A - 0.3356 B + 0.1722 C + 0.2419 AB - 0.2130 BC - 0.1301ABC \quad (15)$$

As shown in Fig. 4h, i, the Young's modulus and tensile strength of the NF membranes were significantly increased with raising the CA concentration (p -value < 0.05). In a study conducted by ElMessiry and Fadel [42], it was found that the increase of the CA percentage in the CA/poly (vinyl chloride) composite NF improved the tensile properties. The improvement in the mechanical properties of NF was due to stiffening the molecular networks, which was, in turn, owing to the formation of intermolecular hydrogen bonds that restricted the movement of the molecular chain, as explained in the FTIR analysis presented in the next section. In contrast, the UTS and Young's modulus were decreased as the drug/polymer ratio was increased (p -value < 0.05), which was consistent with the results shown in the previous work (Fig. 4h, i). The reason for this could be the reduction of the physical interaction between polymer chains and the changes of the NF microstructure resulting from the addition of SF in the polymeric solution. In agreement with our finding, Farzamfar et al. [43] also showed that the increased concentration of taurine reduced the UTS of NF.

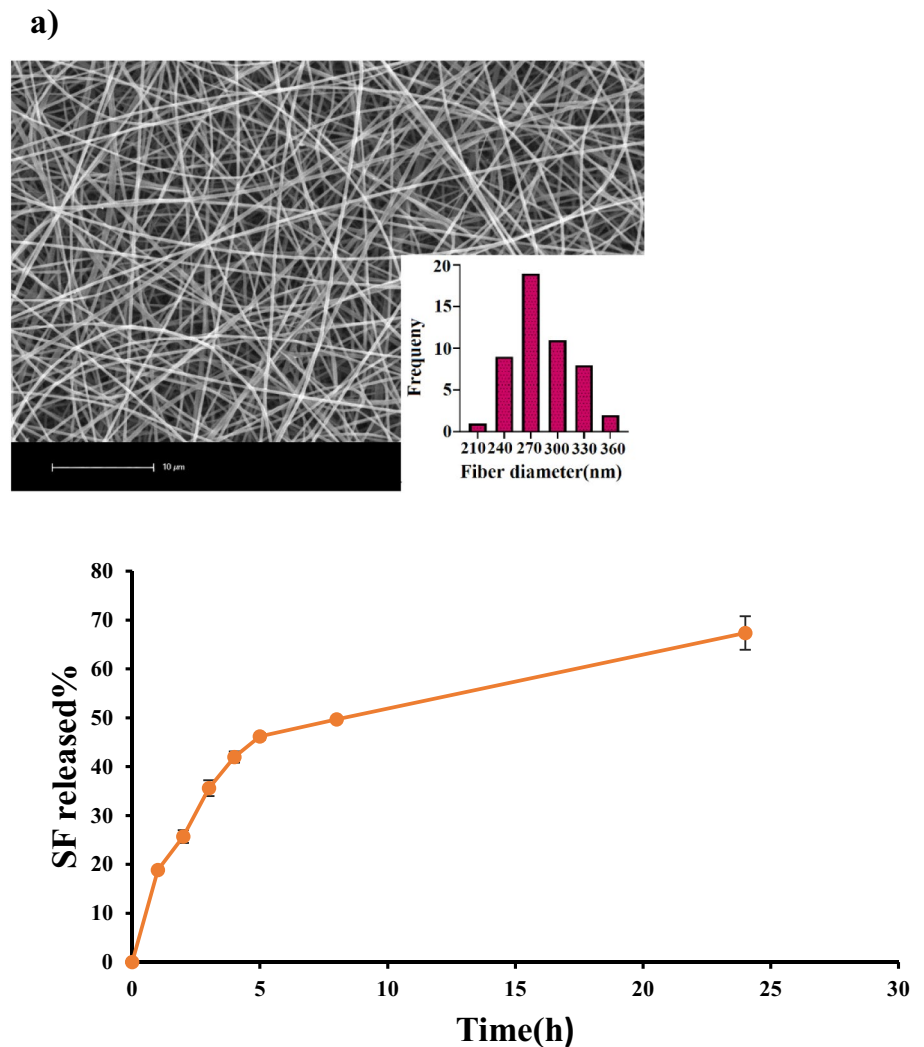
Optimization

The optimized NF was sensibly selected based on measures such as smaller diameter, higher DL%, EE%, RE%, UTS, and Young's modulus. The formulation contained 12%w/v blend ratio of (20/80 w/w) PCL/CA, and 7.2% w/w SF was

Table 5 Comparative levels of predicted and observed responses for the optimized formulation (means ± S.D.; $n = 3$)

Responses	Diameter (nm)	Encapsulation efficiency (%)	Drug loading (%)	Release efficiency (%)	Ultimate tensile strength (MPa)	Young’s modulus (MPa)
Predicted value	294.628	97.2159	7.23472	53.4295	1.11377	76.9509
Experiment value	281.44 ± 32.85	97.96 ± 1.38	7.48 ± 0.105	51.05 ± 0.93	1.08 ± 0.13	74.96 ± 1.44
Error%	4.476	-0.7613	-3.459	4.447	3.032	2.587

Fig. 5 **a** SEM image of SF-loaded optimized NF. **b** In vitro release profile of optimized SF-loaded NF. Each point represents the mean ± SD of three experiments



selected as the optimized formulation by the desirability of 66%. This formulation was developed and characterized for the response variables. As shown in Table 5, the predicted values for the responses were in a good agreement with the obtained results, representing the reliability of

the optimization process. The shape of the SF-loaded optimized NF is shown in Fig. 5a, revealing that the optimized NFs were bead-free, uniform, cylindrical, and smooth fibers. The in vitro release profile of the optimized SF-loaded NF is shown in Fig. 5b. The release data of the optimized

Table 6 Correlation coefficient (R^2) achieved from curve fitting of mean SF release data ($n = 3$) from optimized NF

Formulation	Kinetic models (R^2)			Korsmeyer-Peppas parameters		
	Baker-Lonardale	Higuchi	First order	Zero order	n	R^2
SF-loaded hybrid NF	0.9464	0.9022	0.8852	0.7713	0.4056	0.9313

Fig. 6 FTIR spectra of **a** CA, **b** PCL, **c** SF, **d** SF-free hybrid NF, **e** SF-loaded hybrid NF

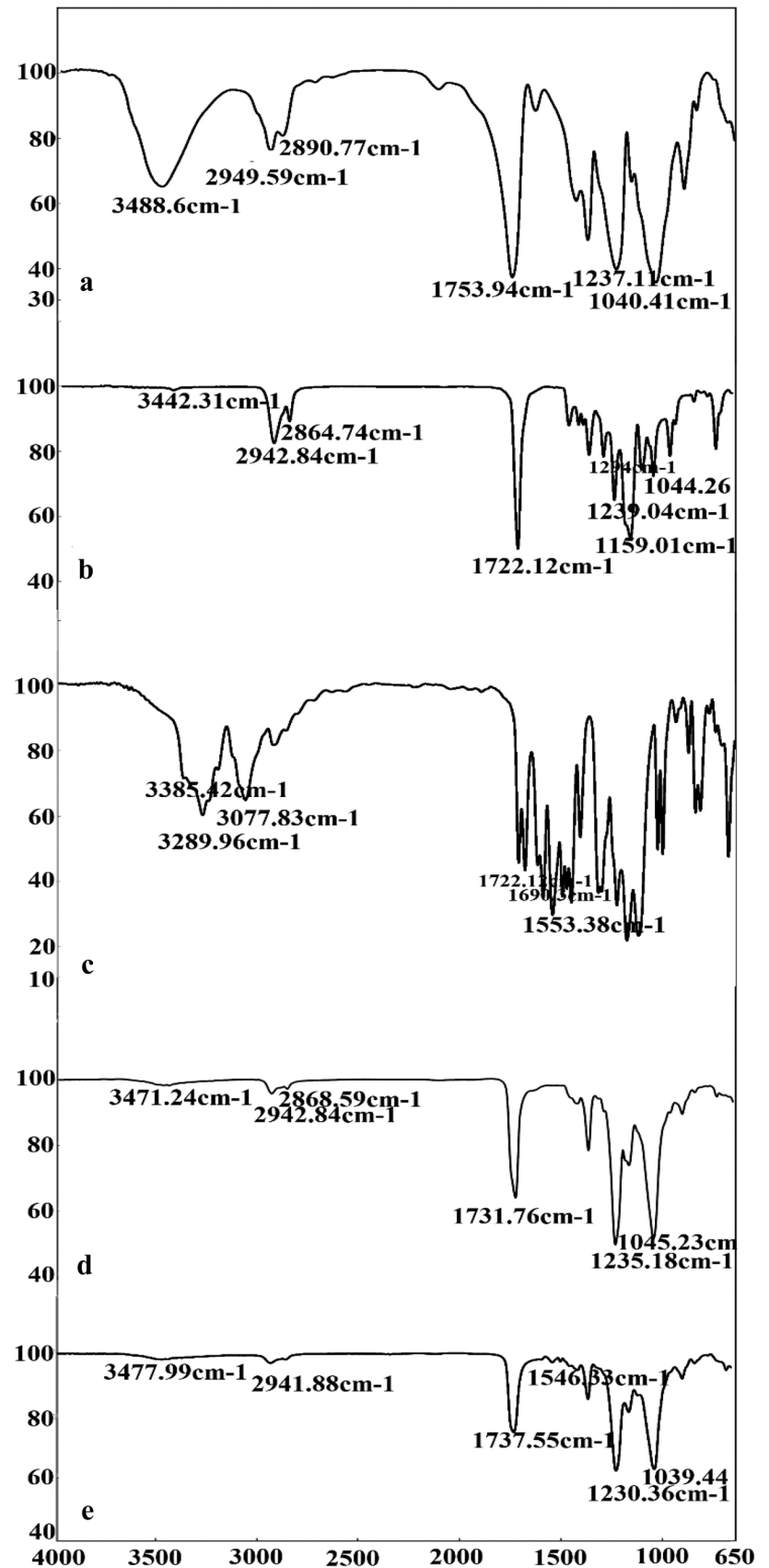


Fig. 7 XRD patterns
a PCL **b** CA **c** SF **d** SF-free
NF **e** SF-loaded NF

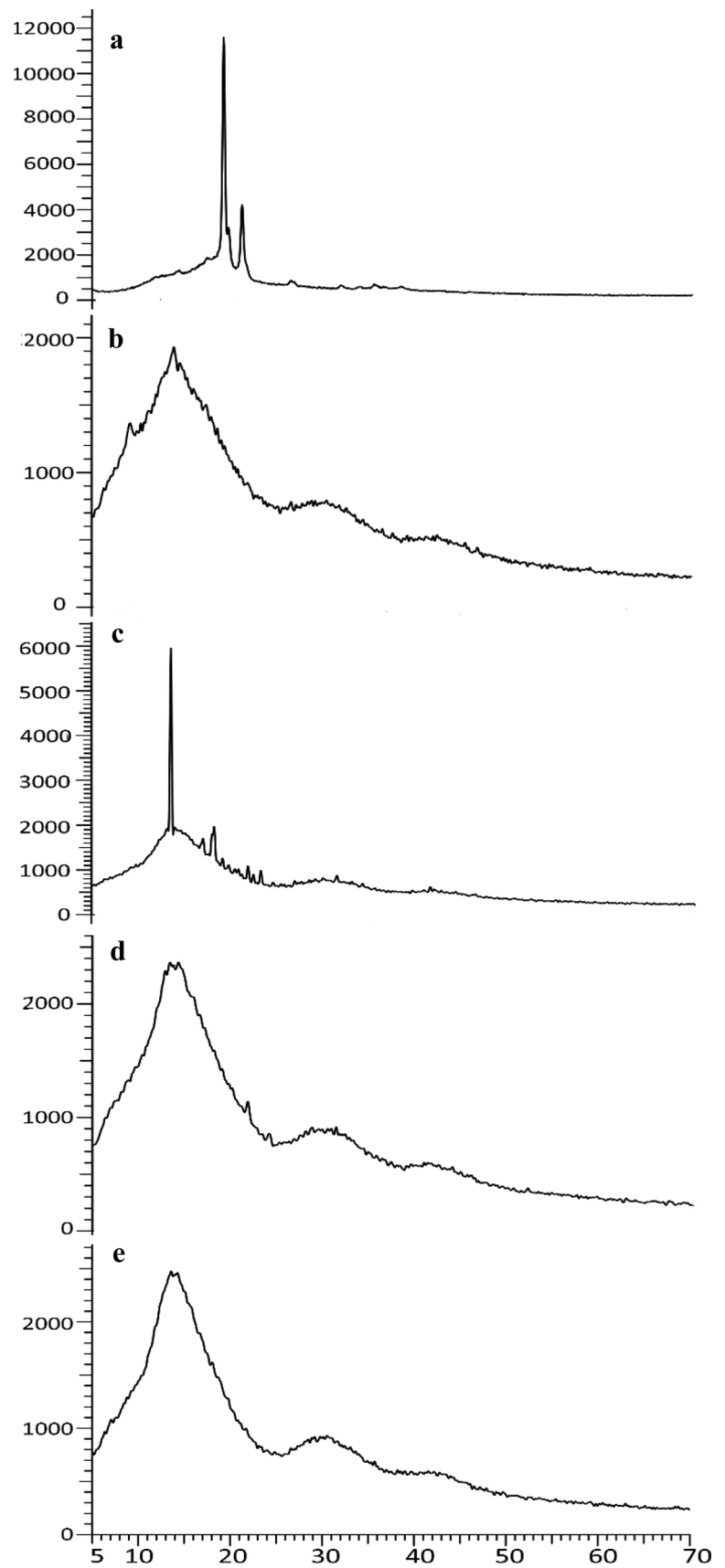
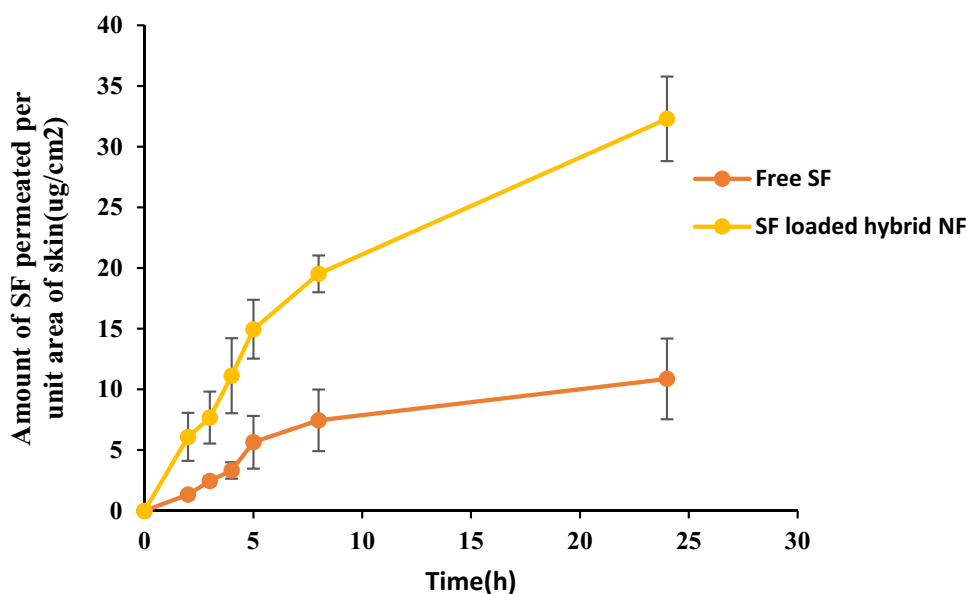


Fig. 8 Skin permeation profile of SF permeated from SF-loaded hybrid NF and SF suspension. Each point represents the mean \pm SD of 3 experiments



formulation within 24 h was analyzed by different kinetic models. The results of the correlation coefficient are shown in Table 6. According to the best fit with the highest correlation (R^2) value, it could be concluded that the optimized formulation followed the Baker-Lonsdale model with the R^2 value of 0.9464. As shown in Table 6, the obtained n value was 0.4056, which was less than the 0.45 value. The magnitude of the n value suggested that Fickian diffusion mechanism was the main mechanism that released the drug from the polymer bed.

FTIR spectroscopy

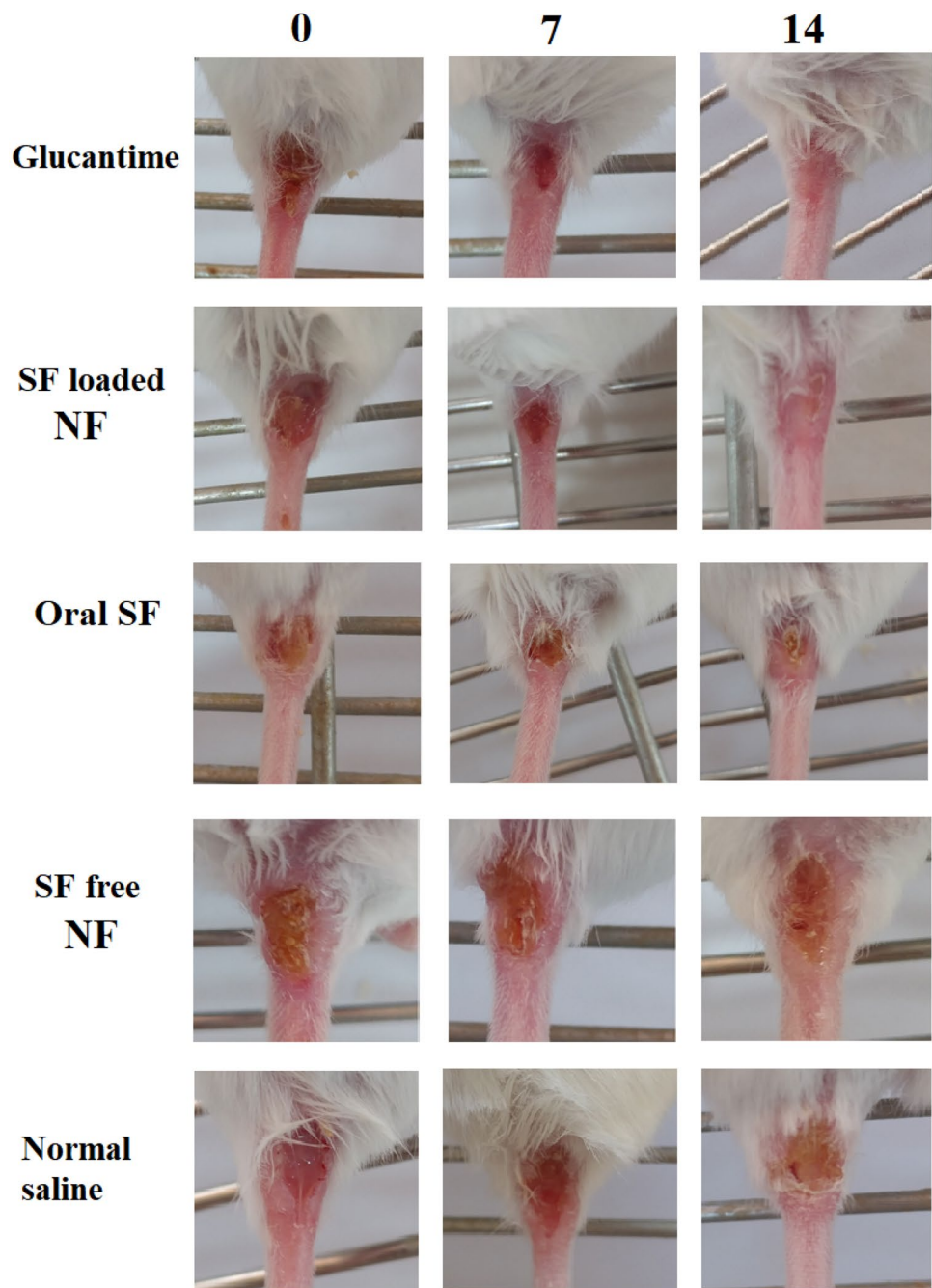
The FTIR spectra of CA, PCL, SF, and NF with and without SF are shown in Fig. 6. In the FTIR spectrum of the CA polymer, these peaks included the following: O–H group at 3488.6 cm^{-1} , CH_2 stretching at 2949.59 and 2890.77 cm^{-1} , COO stretching vibrations at 1753.94 cm^{-1} , and C–O–C bonds at 1040.41 and 1237.11 cm^{-1} [44]. The FTIR spectra of PCL showed the small peaks at 2864.74 cm^{-1} and 2942.84 cm^{-1} , which belonged to the stretching vibrations of CH_2 . The sharp peak at 1722.12 cm^{-1} indicated the stretching vibrations of the C=O group, and the stretching vibrations of the C–O–C group were represented in 1000 – 1300 cm^{-1} [45]. In the FTIR spectrum of SF, the peaks at 3385.42 and 3289.96 cm^{-1} belonged to the N–H stretching. The peak at 3077.63 cm^{-1} could be attributed to the C–H stretching band and that at 1722.12 cm^{-1} was due to the C=O bond of the buried group. Besides, the peak at 1690.3 cm^{-1} referred to the C=O bond of the amide group.

On the other hand, the bands at 1400 – 1600 cm^{-1} were due to the presence of the C=C and C=N stretching [46]. In the FTIR spectra of PCL-CA NF, several characteristics peaks of both PCL and CA were detected. As can be seen, the carbonyl stretching of the composite NF was shifted to 1731.76 cm^{-1} , which might be due to hydrogen bonds formed between the polymer chains. In the FTIR of the SF-loaded hybrid NF, although all characteristics peaks of SF were not seen in the spectrum because SF was low in the fiber, the presence of SF was confirmed by the absorption band at 1505 and 1546.63 cm^{-1} , which corresponded to the C=N stretching.

X-ray diffraction (XRD) analysis

In order to evaluate the physical features of SF and other components in NF, XRD investigations were performed. Figure 7 shows the XRD patterns of SF, PCL, CA, and optimized NF with and without SF. As shown in Fig. 7a, the pure PCL displayed two sharp peaks at 2θ of 21.3° and 23.6° , which were consistent with the previous studies [47]. For CA, one diffraction halo was observed, indicating that the polymer was amorphous (Fig. 7b) [48]. In the XRD spectrum of SF, many sharp peaks could be seen, thus evidencing the crystalline structure of SF (Fig. 7c). In the patterns of the drug-free NF, the characteristic reflections of PCL were absent, thus showing the amorphous state of materials in the composite NF, where the original structure of the pure PCL had been lost. This could be due to the short fiber solidification time during the electrospinning process or hydrogen binding in the polymer matrix, hindering

Fig. 9 Representative images of lesion at tail base of mice treated with normal saline, SF-free NF, and SF-loaded NF



the arrangement of macromolecular chains in the NF [49]. In addition, the sharp peaks of SF were absent in PCL-CA NF, thus indicating that SF was converted into an amorphous form in the composite NF or molecularly dispersed in NF.

Skin permeation

The results obtained in regard to the SF skin permeation across shed rat skin can be observed in Fig. 8. PCL-CA composite NF was found to considerably enhance the SF skin permeation, in comparison to the free SF. As shown

in Fig. 8, the SF cumulative amount which was permeated through the skin model following 24-h incubation was $32.29 \pm 3.48 \mu\text{g}/\text{cm}^2$ for the SF-loaded PCL-CA composite NF; in contrast, the amount which was permeated through the skin for the suspension of SF was almost $10.87 \pm 3.32 \mu\text{g}/\text{cm}^2$. NF mats superiority over SF suspension could be ascribed to the SF solubility improvement owing to molecular dispersion within porous NF mats, as verified through PXRD. Further, NF posed high surface area-to-volume ratios and a highly porous nature, leading to a desirable skin penetration ability [18, 50, 51].

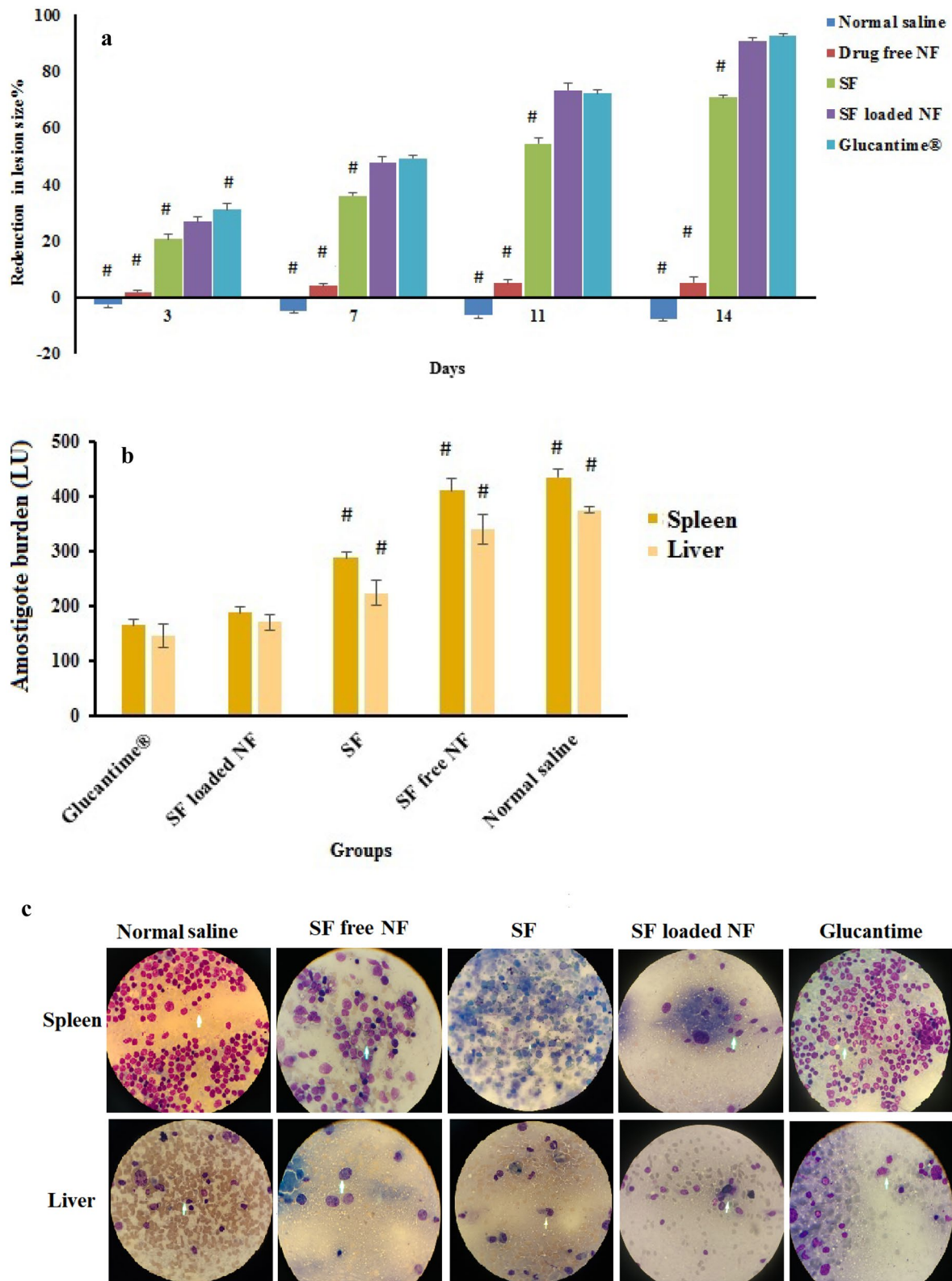


Fig. 10 a Lesion size reduction in mice infected with *L. major* and received different treatments (%). Each point represents the mean \pm SD of at least three experiments. **b** and **c** Parasite burden in the infected liver and spleen of mice infected with *L. major* and received different treatments. **d** The weights of the spleens and livers

of mice infected with parasites in mice and received different treatments. **e** H and E staining images of skin lesions in mice treated with normal saline and SF-loaded hybrid NF. # p value < 0.05 vs. group treated SF-loaded NF. Indicated values are the mean results of 5 BALB/c \pm S.D

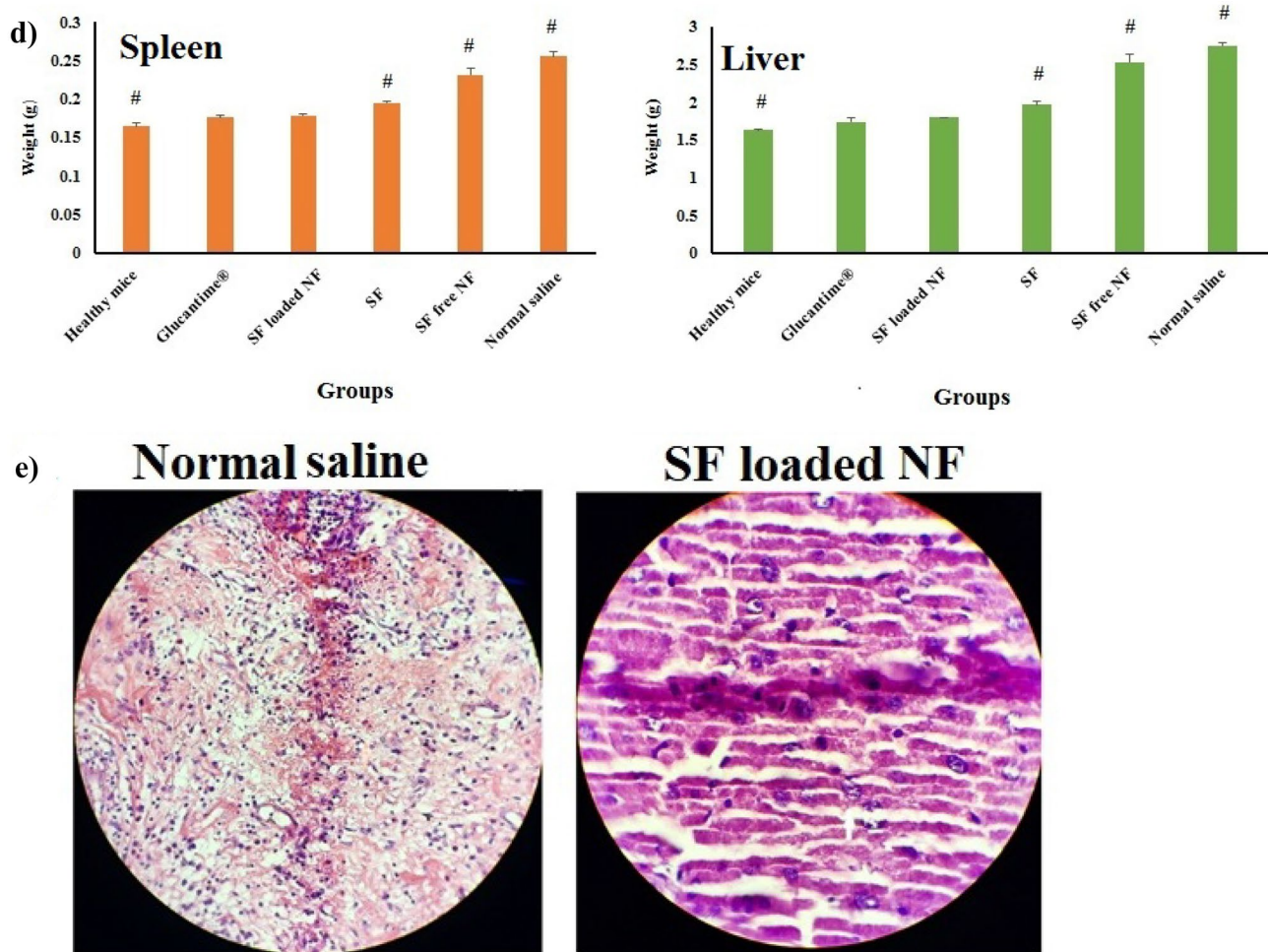


Fig. 10 (continued)

Efficacy studies in *L. major*-infected BALB/C mice

In vivo efficacy of the SF-loaded PCL-CA composite NF was determined in *L. major*-infected mice, as shown in Fig. 9. The effectiveness of each treatment was determined by the calculation of the percentage reduction in the lesion size. The results, as shown in Fig. 10a, indicated that the lesion size was increased in normal saline-treated groups over time. In contrast, a decrease was observed for the orally administered SF, topically administered SF-loaded hybrid NF and Glucantime®. Except for day 3, the SF-loaded hybrid NF resulted in the reduction of the lesion size, similar to the decrease achieved with intraperitoneally administered Glucantime®, which was significantly higher when compared with that obtained with the oral SF. A slight reduction in the size area was also observed in the mice treated with the unloaded NF during the study, which could be triggered by some immunological response caused by the PCL polymer [52]. The parasite burden in the infected liver and spleen was determined. The results

are shown in Fig. 10b, c. The highest parasite burden in the liver and spleen was seen in the negative control group. The parasite number was slightly decreased in the group treated with the drug-free NF, as compared with the negative control one. SF-loaded NF and Glucantime® equally decreased the parasite burden, which was significantly higher than that of the oral SF. As can be seen in Fig. 10d, the weights of the spleen and liver of mice infected with parasites in all groups were increased significantly when compared with those in their healthy counterparts, following the order of normal saline > SF-free NF > oral SF > SF-loaded NF = Glucantime®. More decrease of parasite burdens in the spleen and liver of the mice treated with the SF-loaded NF and Glucantime® was associated with the more decrease of the spleen and liver weight, as compared with other groups. Changes in the body weight of each group under study were also monitored. The weight loss observed in normal saline, the drug-free NF, and oral SF was about $4.53 \pm 1.21\%$, $3.54 \pm 0.45\%$, and $2.18 \pm 0.49\%$, respectively. However, though not

significant, a slight increase in the body weight of mice treated with SF-loaded NF and Glucantime[®] was seen, thus indicating the higher response of animals to this treatment. H and E staining examination also revealed a limited number of amastigotes in the SF-loaded PCL-CA composite NF-treated group, as compared with the normal saline group, thus confirming the local effectiveness of SF in treating leishmania (Fig. 10e). Overall, our in vivo results showed that the leishmanicidal efficacy of the SF-loaded NF was higher than that of the oral SF. This could be considered an advantage of the site-directed delivery of SF with NF, thus enhancing the efficacy of the treatment through increasing and sustaining the drug concentration at the site of action [53, 54].

Conclusion

In this study, the SF-loaded hybrid NF was successfully prepared and physico-chemically characterized. The optimized NF, which was fabricated using the 12%w/v blend ratio of (20/80 w/w) PCL-CA containing 7.2%w/w SF had high EE and released nearly 68% drug during 24 h. According to the obtained results, the fiber diameter was increased with the rise of the polymer concentration, while it was decreased as the concentration of the SF/polymer ratio and CA were increased. The developed SF-loaded hybrid NF showed improved efficacy in vivo by the reduction of the lesion size along with lowering the parasite burden in the liver and spleen in mice infected with *L. major*. The safety and efficacy of this therapy, however, need to be demonstrated in further clinical studies. This will be addressed in our future research.

Contributions

Mahsa Alemomen: investigation, writing; Somayeh Taymouri: conceptualization, investigation, methodology, analysis, writing-review and editing, supervision; Sedigheh Saberi: investigation, methodology, supervision; Jaleh Varshosaz: supervision.

Funding The current research was supported by Research Vice Chancellery of Isfahan University of Medical Sciences (grant number 399358).

Declarations

Ethics approval All experiments were performed as per the guidelines directed by the Ethical Committee of Isfahan University of Medical Sciences in regard to the care and use of laboratory animals (ethics code number # IR.MUI.RESEARCH.REC.1399.489).

Consent for publication All authors are happy with this publication.

Competing interest The authors declare no competing interests.

References

- Bates PA. Transmission of *Leishmania* metacyclic promastigotes by phlebotomine sand flies. *Int J Parasitol.* 2007;37(10):1097–106.
- David CV, Craft N. Cutaneous and mucocutaneous leishmaniasis. *Dermatol Ther.* 2009;22(6):491–502.
- Gupta S, Pal A, Vyas SP. Drug delivery strategies for therapy of visceral leishmaniasis. *Expert Opin Drug Deliv.* 2010;7(3):371–402.
- Peralta MF, Guzman ML, Bracamonte ME, Marco JD, Olivera ME, Carrer DC, et al. Efficacy of topical risedronate and risedronate-Eudragit E complex in a model of cutaneous leishmaniasis induced by *Leishmania (Leishmania) amazonensis*. *Heliyon.* 2021;7(5):e07136.
- Bilgic-Temel A, Murrell DF, Uzun S. Cutaneous leishmaniasis: a neglected disfiguring disease for women. *Int J Women's Dermatol.* 2019;5(3):158–65.
- Esfandiari F, Motazedian MH, Asgari Q, Morowvat MH, Molaei M, Heli H. Paromomycin-loaded mannosylated chitosan nanoparticles: synthesis, characterization and targeted drug delivery against leishmaniasis. *Acta Trop.* 2019;197:105072.
- Shahriyar S, Taymouri S, Saberi S, Asadi P, Tabbakhian M. Preparation and characterization of itraconazole loaded nanomicelles based on dextran-behenic acid for cutaneous leishmaniasis treatment. *Drug Dev Ind Pharm.* 2021;47(3):416–28.
- Wang C-F, Mäkilä EM, Kaasalainen MH, Hagström MV, Salonen JJ, Hirvonen JT, et al. Dual-drug delivery by porous silicon nanoparticles for improved cellular uptake, sustained release, and combination therapy. *Acta Biomater.* 2015;16:206–14.
- Sanderson L, Yardley V, Croft SL. Activity of anti-cancer protein kinase inhibitors against *Leishmania* spp. *J Antimicrob Chemother.* 2014;69(7):1888–91.
- Abou-El-Naga IF, Mady RF, Hussien Mogahed NMF. In vitro effectivity of three approved drugs and their synergistic interaction against *Leishmania infantum*. *Biomedica.* 2020;40:89–101.
- Bondi ML, Botto C, Amore E, Emma MR, Augello G, Craparo EF, et al. Lipid nanocarriers containing sorafenib inhibit colonies formation in human hepatocarcinoma cells. *Int J Pharm.* 2015;493(1–2):75–85.
- Ahiwale RJ, Chellampillai B, Pawar AP. Investigation of novel sorafenib tosylate loaded biomaterial based nano-cochleates dispersion system for treatment of hepatocellular carcinoma. *J Dispers Sci Technol.* 2022;43(10):1568–86.
- Jain S, Tripathi S, Tripathi PK. Invasomes: potential vesicular systems for transdermal delivery of drug molecules. *J Drug Deliv Sci Technol.* 2021;61:102166.
- Van Bocxlaer K, Yardley V, Murdan S, Croft SL. Topical formulations of miltefosine for cutaneous leishmaniasis in a BALB/c mouse model. *J Pharm Pharmacol.* 2016;68(7):862–72.
- Zamani M, Prabhakaran MP, Ramakrishna S. Advances in drug delivery via electrospun and electrosprayed nanomaterials. *Int J Nanomedicine.* 2013;8:2997.
- Abid S, Hussain T, Raza ZA, Nazir A. Current applications of electrospun polymeric nanofibers in cancer therapy. *Mater Sci Eng C.* 2019;97:966–77.
- Kataria K, Gupta A, Rath G, Mathur RB, Dhakate SR. In vivo wound healing performance of drug loaded electrospun composite nanofibers transdermal patch. *Int J Pharm.* 2014;469(1):102–10.
- Goyal R, Macri LK, Kaplan HM, Kohn J. Nanoparticles and nanofibers for topical drug delivery. *J Control Release.* 2016;240:77–92.

19. Esentürk İ, Balkan T, Özhan G, Döşler S, Güngör S, Erdal MS, et al. Voriconazole incorporated nanofiber formulations for topical application: preparation, characterization and antifungal activity studies against *Candida* species. *Pharm Dev Technol.* 2020;25(4):440–53.
20. Alishahi M, Khorram M, Asgari Q, Davani F, Goudarzi F, Emami A, et al. Glucantime-loaded electrospun core-shell nanofibers composed of poly (ethylene oxide)/gelatin-poly (vinyl alcohol)/chitosan as dressing for cutaneous leishmaniasis. *Int J Biol Macromol.* 2020;163:288–97.
21. Rahimi M, Tabaei SJS, Ziai SA, Sadri M. Anti-leishmanial effects of chitosan-polyethylene oxide nanofibers containing berberine: an applied model for leishmania wound dressing. *Iran J Med Sci.* 2020;45(4):286.
22. Khan G, Patel RR, Yadav SK, Kumar N, Chaurasia S, Ajmal G, et al. Development, optimization and evaluation of tinidazole functionalized electrospun poly (ϵ -caprolactone) nanofiber membranes for the treatment of periodontitis. *RSC Adv.* 2016;6(102):100214–29.
23. Khan G, Yadav SK, Patel RR, Kumar N, Bansal M, Mishra B. Tinidazole functionalized homogeneous electrospun chitosan/poly (ϵ -caprolactone) hybrid nanofiber membrane: Development, optimization and its clinical implications. *Int J Biol Macromol.* 2017;103:1311–26.
24. Zhijiang C, Yi X, Haizheng Y, Jia J, Liu Y. Poly (hydroxybutyrate)/cellulose acetate blend nanofiber scaffolds: preparation, characterization and cytocompatibility. *Mater Sci Eng C.* 2016;58:757–67.
25. Unnithan AR, Gnanasekaran G, Sathishkumar Y, Lee YS, Kim CS. Electrospun antibacterial polyurethane–cellulose acetate–zein composite mats for wound dressing. *Carbohydr Polym.* 2014;102:884–92.
26. Samadian H, Zamiri S, Ehterami A, Farzamfar S, Vaez A, Khastar H, et al. Electrospun cellulose acetate/gelatin nanofibrous wound dressing containing berberine for diabetic foot ulcer healing: in vitro and in vivo studies. *Sci Rep.* 2020;10(1):1–12.
27. Hou J, Sun X, Zhang W, Li L, Teng H. Preparation and characterization of electrospun fibers based on poly (L-lactic acid)/cellulose acetate. *Chinese J Polym Sci.* 2012;30(6):916–22.
28. Vatankhah E. Rosmarinic acid-loaded electrospun nanofibers: in vitro release kinetic study and bioactivity assessment. *Eng Life Sci.* 2018;18(10):732–42.
29. Kar S, Sharma G, Das PK. Fucoidan cures infection with both antimony-susceptible and-resistant strains of *Leishmania donovani* through Th1 response and macrophage-derived oxidants. *J Antimicrob Chemother.* 2011;66(3):618–25.
30. Maheshwari SU, Kumar SV, Nagiah N, Uma TS. Electrospinning of polyvinylalcohol–polycaprolactone composite scaffolds for tissue engineering applications. *Polym Bull.* 2013;70(11):2995–3010.
31. Herrero-Herrero M, Gómez-Tejedor J-A, Vallés-Lluch A. PLA/PCL electrospun membranes of tailored fibres diameter as drug delivery systems. *Eur Polym J.* 2018;99:445–55.
32. Zahedi P, Rezaeian I, Jafari SH, Karami Z. Preparation and release properties of electrospun poly (vinyl alcohol)/poly (ϵ -caprolactone) hybrid nanofibers: optimization of process parameters via D-optimal design method. *Macromol Res.* 2013;21(6):649–59.
33. Moradkhannejhad L, Abdouss M, Nikfarjam N, Shahriari MH, Heidary V. The effect of molecular weight and content of PEG on in vitro drug release of electrospun curcumin loaded PLA/PEG nanofibers. *J Drug Deliv Sci Technol.* 2020;56:101554.
34. Taymouri S, Hashemi S, Varshosaz J, Minaiyan M, Talebi A. Fabrication and evaluation of hesperidin loaded polyacrylonitrile/polyethylene oxide nanofibers for wound dressing application. *J Biomater Sci Polym Ed.* 2021;32(15):1944–65.
35. Alavarse AC, de Oliveira Silva FW, Colque JT, da Silva VM, Prieto T, Venancio EC, et al. Tetracycline hydrochloride-loaded electrospun nanofibers mats based on PVA and chitosan for wound dressing. *Mater Sci Eng C.* 2017;77:271–81.
36. Eskitoros-Togay ŞM, Bulbul YE, Tort S, Korkmaz FD, Acartürk F, Dilsiz N. Fabrication of doxycycline-loaded electrospun PCL/PEO membranes for a potential drug delivery system. *Int J Pharm.* 2019;565:83–94.
37. Chen SC, Huang XB, Cai XM, Lu J, Yuan J, Shen J. The influence of fiber diameter of electrospun poly (lactic acid) on drug delivery. *Fibers Polym.* 2012;13(9):1120–5.
38. Kaur D, Dhakate SR, Gupta A. Anti-emetic drug delivery for cancer patients through electrospun composite nanofibers transdermal patch: in vitro study. *Adv Mater Lett.* 2015;6(1):33–9.
39. Zupančič Š, Potrč T, Baumgartner S, Kocbek P, Kristl J. Formulation and evaluation of chitosan/polyethylene oxide nanofibers loaded with metronidazole for local infections. *Eur J Pharm Sci.* 2016;95:152–60.
40. Zamani M, Morshed M, Varshosaz J, Jannesari M. Controlled release of metronidazole benzoate from poly ϵ -caprolactone electrospun nanofibers for periodontal diseases. *Eur J Pharm Biopharm.* 2010;75(2):179–85.
41. Ramos DM, Abdulmalik S, Arul MR, Rudraiah S, Laurencin CT, Mazzocca AD, et al. Insulin immobilized PCL-cellulose acetate micro-nanostructured fibrous scaffolds for tendon tissue engineering. *Polym Adv Technol.* 2019;30(5):1205–15.
42. ElMessiry M, Fadel N. The tensile properties of electrospun poly vinyl chloride and cellulose acetate (PVC/CA) bi-component polymers nanofibers. *Alexandria Eng J.* 2019;58(3):885–90.
43. Farzamfar S, Naseri-Nosar M, Samadian H, Mahakizadeh S, Tajerian R, Rahmati M, et al. Taurine-loaded poly (ϵ -caprolactone)/gelatin electrospun mat as a potential wound dressing material: in vitro and in vivo evaluation. *J Bioact Compat Polym.* 2018;33(3):282–94.
44. Ullah A, Saito Y, Ullah S, Haider MK, Nawaz H, Duy-Nam P, et al. Bioactive Sambong oil-loaded electrospun cellulose acetate nanofibers: preparation, characterization, and in-vitro biocompatibility. *Int J Biol Macromol.* 2021;166:1009–21.
45. Khoshbakht S, Asghari-Sana F, Fathi-Azarbayjani A, Sharifi Y. Fabrication and characterization of tretinoin-loaded nanofiber for topical skin delivery. *Biomater Res.* 2020;24(1):1–7.
46. Nasehi N, Varshosaz J, Taymouri S, Rostami M, Akbari V, Firoozpour L. Sorafenib loaded pluronic F127-lithocholic acid micelles for prostate cancer therapy: formulation, optimization, and in vitro evaluation against LNCaP cells. *Int J Polym Mater Polym Biomater.* 2020;69(3):158–72.
47. Aghdam RM, Najarian S, Shakhesi S, Khanlari S, Shaabani K, Sharifi S. Investigating the effect of PGA on physical and mechanical properties of electrospun PCL/PGA blend nanofibers. *J Appl Polym Sci.* 2012;124(1):123–31.
48. Yu D-G, Li X-Y, Wang X, Chian W, Liao Y-Z, Li Y. Zero-order drug release cellulose acetate nanofibers prepared using coaxial electrospinning. *Cellulose.* 2013;20(1):379–89.
49. Lu H, Wang Q, Li G, Qiu Y, Wei Q. Electrospun water-stable zein/ethyl cellulose composite nanofiber and its drug release properties. *Mater Sci Eng C.* 2017;74:86–93.
50. Kamble RN, Gaikwad S, Maske A, Patil SS. Fabrication of electrospun nanofibres of BCS II drug for enhanced dissolution and permeation across skin. *J Adv Res.* 2016;7(3):483–9.
51. Song J, Fan X, Shen Q. Daidzein-loaded nanostructured lipid carriers-PLGA nanofibers for transdermal delivery. *Int J Pharm.* 2016;501(1–2):245–52.
52. McLoughlin CE, Smith MJ, Auttachoat W, Bowlin GL, White KL. Evaluation of innate, humoral and cell-mediated immunity in mice following in vivo implantation of electrospun polycaprolactone. *Biomed Mater.* 2012;7(3):35015.
53. Van Bocxlaer K, Gaukel E, Hauser D, Park SH, Schock S, Yardley V, et al. Topical treatment for cutaneous leishmaniasis: dermatopharmacokinetic lead optimization of benzoxaboroles. *Antimicrob Agents Chemother.* 2018;62(5):e02419–e2517.

54. Santos CM, de Oliveira RB, Arantes VT, Caldeira LR, de Oliveira MC, Egito ES, et al. Amphotericin B-loaded nanocarriers for topical treatment of cutaneous leishmaniasis: development, characterization, and in vitro skin permeation studies. *J Biomed Nanotechnol.* 2012;8(2):322–9.

Springer Nature or its licensor holds exclusive rights to this article under a publishing agreement with the author(s) or other rightsholder(s); author self-archiving of the accepted manuscript version of this article is solely governed by the terms of such publishing agreement and applicable law.

Publisher's Note Springer Nature remains neutral with regard to jurisdictional claims in published maps and institutional affiliations.